OFFICE OF NAVAL RESEARCH

GRANT or CONTRACT: N00014-91J-1201

R&T CODE: 4133032
Richard Carlin

TECHNICAL REPORT NO. 29

"New Highly-Sensitive Methods for Electroanalytical Chemistry Based on Nanotubule
Membranes"

Yoshio Kobayashi and Charles R. Martin

Prepared for Publication

in

Analytical Chemistry

Colorado State University
Department of Chemistry
Fort Collins, CO 80523-1872

June 1, 1999

19990706 134

REPORT DOCUMENTATION PAGE

1. June 1, 1999

2. Interim report

3. "New Highly-Sensitive Methods for Electroanalytical Chemistry Based on Nanotubule Membranes"

4. GRANT: N00014-91J-1201, R&T CODE: 4133032

5. Yoshio Kobayashi and Charles R. Martin

6. Charles R. Martin, Department of Chemistry, Colorado State University, Fort Collins, CO 80523-1872

7. TECHNICAL REPORT NO. 29

8. Office of Naval Research, Chemistry Division, 800 North Quincy Street, Arlington, VA 22217-5660

9. To be published in *Analytical Chemistry*

11. Abstract: Two new methods of electroanalysis are described. These methods are based on membranes containing monodisperse Au-nanotubules with inside diameters approaching molecular dimensions (~ 1 to ~ 3 nm). In one method the analyte species is detected by measuring the change in trans-membrane current when the analyte is added to the nanotubule-based cell. The second method entails the use of a concentration cell based on the nanotubule membrane. In this case the change in membrane potential is used to detect the analyte. Detection limits as low as 10^{-11} have been achieved. Hence, these methods compete with even the most sensitive of modern analytical methodologies. In addition, excellent molecular-sized-based selectivity is observed.

12. Subject terms: Nanotubule membranes, ultratrace analysis, electroanalytical chemistry

17. 18. 19. Unclassified

New Highly-Sensitive Methods for Electroanalytical Chemistry Based on Nanotubule Membranes

Yoshio Kobayashi and Charles R. Martin*
Department of Chemistry
Colorado State University
Ft. Collins, CO 80523

*Corresponding author via E-mail at crmartin@lamar.colostate.edu

Abstract

Two new methods of electroanalysis are described. These methods are based on membranes containing monodisperse Au nanotubules with inside diameters approaching molecular dimensions. In one method the analyte species is detected by measuring the change in trans-membrane current when the analyte is added to the nanotubule-based cell. The second method entails the use of a concentration cell based on the nanotubule membrane. In this case the change in membrane potential is used to detect the analyte. Detection limits as low as 10^{-11} M have been achieved. Hence, these methods compete with even the most sensitive of modern analytical methodologies. In addition, excellent molecular-sized-based selectivity is observed.

INTRODUCTION

We have recently described a family of membranes that contain Au nanotubules with inside diameters of molecular dimensions (e.g., <1 nm).[1-3] These membranes are prepared via the template method,[4] by electrolessly plating Au within the pores of a microporous filtration membrane.[5] Because of the extremely small inside diameters of the Au nanotubules, these membranes can be used to cleanly separate small molecules on the basis of molecular size.[2] Charge-based[1] and chemically-based[3] transport selectivity can also be introduced into these membranes.

In addition to possible applications in membrane-based chemical separations[2,3], we have recently presented preliminary data that suggest that such membranes might form the basis for new and highly sensitive methods of electroanalysis.[6] In this case the nanotubule membrane separates two salt solutions, a constant trans-membrane potential is applied, and the resulting trans-membrane current is measured. When an analyte species with molecular dimensions comparable to the inside diameter of the nanotubules is introduced into this cell, the trans-membrane current decreases; the magnitude of the change in current is proportional to the concentration of the analyte species.[6] Detection limits as low as 10^{-9} M were achieved in our preliminary report.[6]

We have since conducted a series of fundamental investigations aimed at exploring the effects of electrodes and electrolytes used, nanotubule inside diameter, and molecular size and charge of the analyte on the detection limits achievable with this new electroanalytical cell. These investigations have allowed us to achieve electroanalytical detection limits as low as 10^{-11} M. In addition, we have developed a second nanotubule-based method of electroanalysis that entails measurement of trans-membrane potential in a

concentration cell based on the nanotubule membranes. Detection limits as low as 10^{-10} were achieved. Results of these investigations are described here.

EXPERIMENTAL

Materials.   Anhydrous $SnCl_2$, CF_3COOH, poly(vinylpyrrolidone) (MW = 24,000), and silver wire (purity = 99.99 %, thickness = 1 mm) were obtained from Aldrich and were used as received. Anhydrous KF (Baker), CH_3OH, HCHO, $NaHCO_3$, KCl, KI (Fisher), Na_2SO_3, NH_4OH, H_2SO_4 (Mallinckrodt), pyridine (Fisher), $AgNO_3$ (Spectrum), and gold electroless plating solution, Oromerse Part B (Technic Inc.) were used as received. Quinine (Sigma), $Ru(bpy)_3^{2+}$ dichloride (bpy = (2,2'-bipyridine), GFS), 2-naphthol (Aldrich), bromocresol green (BCG) (Baker), sodium tetraphenylborate (TPB^-) (Aldrich), and methyl viologen (MV^{2+}) dichloride hydrate (Aldrich) were used as the analyte molecules. The structures and approximate sizes of these various analytes are shown in Figure 1. Milli Q 18-MΩ water was used to make all solutions. Track-etched polycarbonate filters (Osmonics) were used as the template membranes. These membranes contain cylindrical pores (6×10^8 pores cm^{-2}) with a uniform diameter of 30 nm running through the complete thickness (6 μm) of the membrane.

Preparation of the Au nanotubule membranes.   An electroless plating procedure, similar to that described previously,[5] was used to deposit the Au nanotubules within the pores of the template membrane. The template membrane was washed with methanol and then immersed for 45 min in 50 % (v/v) methanol/water that was 0.026 M in $SnCl_2$ and 0.07 M in CF_3COOH. This resulted in deposition of the "sensitizer" (Sn^{2+})[5] onto all membrane surfaces (both the pore walls and the membrane faces). The membrane was rinsed with methanol for 5 min and immersed into an aqueous solution of ammonical $AgNO_3$ (0.035 M) for 5 min. This resulted in the deposition of nanoparticles of Ag on all membrane surfaces. The membrane was then rinsed with water.

The standard plating bath used for these studies was a mixture consisting of 20 mL of aq. 0.025 M $NaHCO_3$, 0.5 mL of Oromerse Part B, 0.32 g of Na_2SO_3, and 1.1 g

of a 40 % formaldehyde aqueous solution (the reducing agent). The Au(I) concentration in this standard bath was 7.7×10^{-3} M and the pH was 12. Prior to immersion of the template membrane, the pH was decreased to pH=10 by drop-wise addition of 0.5 M H_2SO_4. This lower pH value results in slower, and thus more uniform, Au deposition.[2] Au plating was done at 5 °C for a duration of 12 hr. After plating, the membrane was washed with water and then dried at room temperature. In addition to depositing the Au nanotubules within the pores, Au films are deposited onto both faces of the template membrane; these surface films were removed by simply applying and then removing a strip of tape (Highland brand invisible tape # 6200).[5]

This standard plating bath yielded nanotubules with approximate inside dia. (as determined via gas-permeation measurements, *vide infra*) of 2.8 nm. To make larger diameter nanotubules, the 20 mL of aqueous 0.025 M $NaHCO_3$ was replaced with 20 mL of water. The initial pH of this plating bath was 10; however, during the course of the 12 hr (5 °C) plating process the pH drops to 9.6, and this causes the rate of the plating reaction to decrease. This modified plating bath yielded nanotubules with diameters of ~3.8 nm.

A second modified plating bath was used to make smaller diameter nanotubules. The 20 mL of aqueous 0.025 M $NaHCO_3$ was again replaced with 20 mL of water, and H_2SO_4 was not subsequently added to the bath. This resulted in a plating bath of pH = 12 and faster plating rates. Again, plating was done for 12 hr at 5 °C. This modified plating bath yielded nanotubules of diameter ~2.2 nm.

Two other procedures were used to make smaller diameter nanotubules. In the first, a nanotubule membrane obtained from the standard plating bath was thermally treated at 160 °C for 6 h in air. We have shown that this causes the template membrane to shrink[5]; after this heat-treatment, the gas-permeation method yielded a nanotubule inside diameter of ~1.4 nm. The second method entailed subjecting the nanotubule membranes obtained from the first plating bath to a second plating

treatment in the same bath. After the first plating, the surface Au films were removed and the membrane was immersed into a methanolic solution that was 1 wt% in poly(vinylpyrrolidone). After rinsing with methanol, the membrane was plated a second time in the standard plating bath. This resulted in nanotubules of diameter ~1.8 nm.

Gas-transport measurements. The inside diameter of the Au nanotubules plated within the template membranes was determined using a gas-permeation method.[7] The gas-transport cell has been described previously.[8] After placing the Au nanotubule membrane between the upper and lower half-cells, both half-cells were evacuated. The upper half-cell was then pressurized with H2 gas (34.7 PSI). The change of the pressure (P) with time (t) in the lower half-cell was then monitored using a pressure transducer and a strip-chart recorder. The gas flux was determined from the linear portion of the P vs. t transient.[8] The nanotubule diameter was calculated from the experimental flux, the known membrane thickness and the known pore density. [1-3,7]

Electrochemical measurements. A U-tube cell was assembled with the nanotubule membrane separating the two halves of the cell. The membrane was first sandwiched between two pieces of strapping tape (3M Scotch brand # 375); each piece of tape had a hole punched in it (diameter = 6.35 mm). These holes defined the area of the membrane through which the ionic current was passed. The two half-cells were filled with the desired electrolyte (100 mL) and an electrode was placed into each half cell.

Three different sets of electrodes and electrolytes were used. The distance between the electrodes was always 12 cm. The first set consisted of two Pt plate electrodes (2.54 cm^2); the electrolyte used in both half-cells for these electrodes was 0.1 M KF. The second set consisted of two Ag/AgCl wires (diameter = 1 mm, length = 8 cm); the electrolyte used in both half-cells was 0.1 M KCl. The third set consisted of two Ag/AgI wires (diameter = 1 mm, length = 8 cm) immersed in 0.1 M KI. The Ag/AgCl and Ag/AgI wires were prepared as follows[9]: Ag wires were first cleaned by immersion in 3 M HNO3 and rinsed thoroughly with water. The Ag wires were then used as

anodes (Pt plate cathode) in either 0.1 M KCl or KI solution. The desired Ag salt was deposited on the Ag wire by passing a current of 0.4 mA cm^{-2} for 12 hr.

The experimental method used with these cells was to immerse the electrodes into the appropriate electrolyte and apply a constant potential between the electrodes. The resulting trans-membrane current was measured and recorded on an X-t recorder. After obtaining this baseline current, the anode half-cell was spiked with a known quantity of the desired analyte (Figure 1). This results in a decrease in the trans-membrane current. As shown in Figure 2, the current drops rapidly at first and then decreases at a progressively slower rate at longer times. In order to quantify the drop in current, the roughly linear portion of the i vs. t transient between 3 to 5 minutes was extrapolated to t = 0, and Δi was quantified as shown in Figure 2C.

The detection limit was defined as that concentration which produced a Δi twice as large as the noise in the baseline signal. As shown in Figure 2A, the magnitude of the noise (peak-to-peak) is ~ 40 nA. A potentiostat (EG&G 273) was used to apply the potential between the electrodes and measure the trans-membrane current. Both electrolyte solutions were stirred during the electrochemical measurement. This type of cell will be referred as the "*constant-potential cell*."

A second type of electrochemical cell - a simple *concentration cell* - was also explored as part of this work. The U-tube cell described above was used; however, in this case, double-junction Ag/AgCl reference electrodes were immersed into each half-cell. The inner electrode was a commercially-available (CH Instruments) Ag/AgCl reference. This reference electrode was inserted into an outer glass tube (10 mm diameter) with a glass frit (10 μm mean pore diameter) sealed to its end. This outer glass tube was filled with either KCl or KI at the desired concentration.

The Au nanotubule membrane was mounted between the two halves of the U-tube cell. The two half-cells were then filled with the same electrolyte (KCl or KI) but at different concentrations. This resulted in the establishment of a steady-state trans-

membrane potential (E_m)[1], which was measured with an electrometer (Keithley 600B) and recorded on a strip-chart recorder. The analyte species was then added to the half-cell containing the lower salt concentration. This resulted in a change in the trans-membrane potential (ΔE); ΔE was plotted vs. the concentration of the analyte added. It is important to point out that the outer tube of the double-junction reference electrode was filled with the same salt at the same concentration as was used in the half-cell into which it was immersed; hence, there was no junction potential between the outer tube and the half-cell solution. This double-junction approach was used to prevent the salt in the inner reference electrode (3.5 M KCl) from contaminating the solutions used in the half-cells.

RESULTS

Detection of analyte species using the constant-potential cell. We were interested in exploring how the following variables - nature of the electrodes and electrolyte, size and charge of the analyte (Figure 1), and inside diameter of the nanotubules - affect the detection limit observed. We begin by describing the effects of electrodes and electrolyte, and size and charge of the analyte, at a constant nanotubule inside diameter of ~2.8 nm.

Figure 3A shows plots of log Δi vs. log[analyte] for the analytes $Ru(bpy)_3^{2+}$, MV^{2+} and quinine (Figure 1) obtained using Ag/AgCl electrodes and 0.1 M KCl as the electrolyte in both half-cells. A trans-membrane potential of 0.5 V proved optimal in this Ag/AgCl/KCl cell. Higher potentials caused unstable trans-membrane currents, and lower potentials resulted in higher (worse) detection limits. The resulting baseline trans-membrane current was 7 μA.

Calibration curves (e.g., Figure 3) are presented here in log-log format because of the large dynamic range (spanning as much as five orders of magnitude in analyte concentration) obtained with the constant-potential cell. Clearly, this log-log format would not be suitable in real analytical applications of this device. The inset in Figure

3A shows a plot of Δi vs. [Ru(bpy)$_3$$^{2+}$] for the lowest three analyte concentrations studied. As is obvious from the log-log plots, the calibration curve in the inset of Figure 3A is not linear. It shows its greatest sensitivity at low concentrations and the response flattens at higher concentrations. This point will be discussed in greater detail below.

The detection limits obtained using the Ag/AgCl/KCl cell are shown in Table I. Two important points should be noted. First, the detection limit for Ru(bpy)$_3$$^{2+}$ is lower in this Ag/AgCl/KCl cell than in the Pt/KF cell. Second, the detection limit decreases as the size of the analyte molecule increases (see Figure 1).

Figure 3B shows analogous plots for the analytes Ru(bpy)$_3$$^{2+}$, MV^{2+} and quinine obtained using Ag/AgI electrodes and 0.1 M KI as the electrolyte in both half-cells; again, a membrane with ~2.8 nm-diameter tubules was used. A trans-membrane potential of 0.35 V was applied, and the baseline trans-membrane current was 7 μA. Note that the detection limits (Table I) for Ru(bpy)$_3$$^{2+}$ and MV^{2+} were lower in this Ag/AgI/KI cell than in the Ag/AgCl/KCl cell. The detection limit for quinine was the same in both cells.

The majority of the quinine in both the KCl and KI solutions is present as the monoprotonated (monocationic) form. (The pH values of the KCl and KI solutions were measured at 5.38 and 6.60, respectively.) Perhaps the reason the detection limits for Ru(bpy)$_3$$^{2+}$ and MV^{2+} are lower in the Ag/AgI/KI cell while the detection limit for quinine is the same in both this cell and the Ag/AgCl/KCl cell has to do with the difference in charge of these analytes (predominately monovalent vs. divalent). To explore this point, the detection limits for a neutral analyte, 2-naphthol, were obtained in both the Ag/AgI/KI and Ag/AgCl/KCl cells. (At these pH values, the vast majority of the naphthol is present as the neutral.) Like quinine the detection limit for this neutral analyte was the same in both cells (10^{-6} M, Table I).

The data in Table I show that the detection limits for the divalent analytes are better in the Ag/AgI/KI cell than in the Ag/AgCl/KCl cell. There are at least two possible

explanations for this result. First, it is well known that both Cl⁻ and I⁻ chemisorb to Au.[10,11] We will show below that the detection limits, in general, become lower as the nanotubule inside diameter is made smaller. Perhaps halide chemisorption closes down the inside diameter of the nanotubule, and because I⁻ is bigger than Cl⁻, this effect is more dramatic in the presence of I⁻. If this explanation is correct, the highest (poorest) detection limit is obtained in the presence of KF (Table I) because F⁻ does not chemisorb to Au.

If this explanation is correct, then pre-exposure of the Au nanotubule membrane to KI should cause the proposed decrease in nanotubule inside diameter (due to I⁻ chemisorption). Subsequent use of this I⁻-adsorbed membrane in the KF electrolyte should then yield the same detection limit as when KI is used as the electrolyte. To test this possibility a nanotubule membrane was exposed to 0.1 M KI for 24 hr and then used with the Pt plate electrodes in 0.1 M KF. The detection limit obtained for $Ru(bpy)_3^{2+}$ (10^{-9} M) was the same as that observed for this Pt/KF cell when KI was not pre-adsorbed.

This indicates that iodide chemisorption is not the cause of the lower detection limits observed in the presence of KI. This conclusion is supported by the fact that the neutral molecule shows the same detection limit in both the Ag/AgI/KI and Ag/AgCl/KCl cells. However, it seems likely that if the nanotube diameter were made sufficiently small, the difference in size between chemisorbed I⁻ and chemisorbed Cl⁻ could contribute to differences in detection limit between the Ag/AgI/KI and Ag/AgCl/KCl cells.

The other possibility is that the cationic analytes come across these nanotubule membranes as ion-pairs. The difference between the detection limits in the Ag/AgI/KI vs. the Ag/AgCl/KCl cells (Table I) would then be due to the difference in size between the iodide vs. the chloride ion-pairs and to the number of anions the analyte carries with it (two for the divalents and one for quinine). It is important to point out that we have already shown[2] that $Ru(bpy)_3^{2+}$ and MV^{2+} do, indeed, come across such membranes

10

as the ion pairs $Ru(bpy)_3(X^-)_2$ and $MV(X^-)_2$ (X^- = anion). So this ion-pair-based explanation for the lower detection limits in the Ag/AgI/KI cell seems the most likely. Apparently the difference between the quinine cation paired with one I^- vs. this cation paired with one Cl^- is not great enough to cause the detection limit for this predominately monovalent analyte to be significantly different in the Ag/AgI/KI vs. the Ag/AgCl/KCl cells (Table I).

The final variable to be investigated is the effect of nanotubule inside diameter on detection limit. To explore this parameter, membranes with nanotubule inside diameters of approximately of 3.8, 2.8, 2.2, 1.8, and 1.4 nm were prepared (see Experimental) and used in the Ag/AgI/KI cell. Calibration curves for the analytes $Ru(bpy)_3^{2+}$, MV^{2+} and quinine were generated as before (i.e., Figure 3), and detection limits were obtained from these calibration curves. A trans-membrane potential of 0.35 V was used for the membranes containing the 3.8, 2.8, 2.2, and 1.8 nm inside-diameter tubules. A higher trans-membrane potential (0.55 V) was needed for the membrane containing the 1.4 nm-diameter tubules. This is because the resistance of these smallest diameter tubules is so large that a very small (70 nA) and noisy baseline trans-membrane current was observed when 0.35 V was applied. Application of 0.55 V increased the baseline trans-membrane current to 200 nA and reduced the noise to an acceptable level.

Figure 4 shows plots of detection limit for three different analytes vs. the nanotubule inside diameter in the membrane used. A minimum in this plot is observed for each of the three analytes. The nanotubule membrane that produces this minimum (best) detection limit depends on the size of the analyte. These molecules decrease in size in the order $Ru(bpy)_3^{2+}$ > quinine > MV^{2+} (Figure 1). The nanotubule membrane that yields the lowest detection limit follows this size order; that is, the nanotubule diameters that produce the lowest detection limit for $Ru(bpy)_3^{2+}$, quinine, and MV^{2+}

are 2.8 nm, 2.2 nm, and 1.8 nm, respectively. For the roughly spherical analytes, the optimal tubule diameter is a little over twice the diameter of the molecule.

Investigations of molecular-size-based selectivity in the constant-potential cell. The data presented thus far show a strong correlation between detection limit and the relative sizes of the nanotube and the analyte molecule (Figure 4). This indicates that the constant-potential device should show molecular-size-based selectivity. This is not surprising because transport studies[2] showed that these membranes have excellent size-based transport selectivity; indeed, these membranes can cleanly separate small molecules on the basis of molecular size. To explore size-based selectivity in the constant-potential cell, a series of solutions was prepared containing decreasing concentrations of the analyte species, but containing a constant (higher) concentration of an interfering species. Because we are interested in molecular-size-based selectivity, the interfering species was smaller than the analyte species. The response of the nanotubule membrane (nanotube diameter = 2.8 nm) to these solutions was then measured starting from lowest to highest concentration of the analyte species.

Figure 6A shows results of such an experiment using pyridine as the interfering species (10^{-4} M) and either $Ru(bpy)_3^{2+}$, MV^{2+} or quinine as the analyte species. Because pyridine is so much smaller, it does not act as a strong interferent for any of these analytes. The detection limits in the presence of 10^{-4} M pyridine were 10^{-10} M for $Ru(bpy)_3^{2+}$, 10^{-6} M for MV^{2+} and 10^{-7} M for quinine, within an order of magnitude of the detection limit with no added interfering species (Table I). Put another way, the constant potential cell can detect 10^{-10} M $Ru(bpy)_3^{2+}$ in the presence of six orders of magnitude higher pyridine concentration. Such selectivity data may be described quantitatively in terms of a selectivity coefficient obtained by ratioing the slopes of the calibration curves for the analyte and interfering species.[12] However, because this constant-potential cell shows essentially no response to the interfering species pyridine,

a selectivity coefficient cannot be calculated. In order to obtain a selectivity coefficient, a better (larger) interfering molecule is required.

Figure 6B shows results of such an experiment when the analyte was $Ru(bpy)_3^{2+}$ and the interfering species was MV^{2+}. Now at low concentrations of analyte, there is a region where the device produces a constant response due to the constant concentration (10^{-4} M) of this interfering species; i.e., the much higher concentration of the MV^{2+} swamps the response of the device. However, as the concentration of $Ru(bpy)_3^{2+}$ increases, there is a concentration regime where the device responds to this analyte species without interference from the MV^{2+} (Figure 6B). This concentration regime begins at concentrations of $Ru(bpy)_3^{2+}$ above 10^{-8} M. That is, the size-based selectivity is such that the larger analyte species, $Ru(bpy)_3^{2+}$, can be detected down to 10^{-8} M in the presence of four orders of magnitude higher concentration of the smaller interfering species, MV^{2+}.

Because this device produces a measurable response to the interferent MV^{2+} (Figure 3B), a selectivity coefficient can be calculated. We define here the selectivity coefficient $K_{bpy/MV}$ as the slope of the calibration curve for the analyte, $Ru(bpy)_3^{2+}$, divided by the slope for the interfering species, MV^{2+} (Figure 3B). This analysis is somewhat problematic because the calibration curves are nonlinear and because the device is not very sensitive to MV^{2+}. However, taking the data from the central part of the $Ru(bpy)_3^{2+}$ calibration curve in Figure 3B gives a slope of ~400 A M^{-1}; dividing by the slope for the MV^{2+} data gives $K_{bpy/MV} = 4,000$.

These experiments show that, in agreement with our transport studies[2], the nanotube membrane-based constant-potential cell can show excellent size-based selectivity. It is important to point out that we have also shown that chemical transport selectivity can be introduced into these membranes.[3] This should provide another route for introducing selectivity into the analytical devices described here. The other important point to note is the extraordinary sensitivity, as defined by the slope of 400 A

13

M^{-1}, that this cell shows at low concentrations for the large analyte species, $Ru(bpy)_3^{2+}$. Finally, while $Ru(bpy)_3^{2+}$ and MV^{2+} may, on the one hand, be viewed simply as prototype analyte and interfering species, in our transport studies[2] we needed to be able to determine trace concentrations of $Ru(bpy)_3^{2+}$ in the presence of much higher concentrations of MV^{2+}. The constant-potential cell described here would have been ideally suited for this analysis.

Concentration-cell detection. As noted above, we have also found that the nanotube membranes can be used in a potentiometric analytical device. A concentration cell was assembled using the 2.8 nm tube-diameter membrane with 1 M KCl on one side and 10^{-5} M KCl on the other side of the membrane. We have previously shown that in the presence of chemisorbed Cl^-, the Au nanotubule membranes can be cation permselective.[1] For this reason, this cell showed a membrane potential of +95 mV. This potential is substantially less than would be obtained for an ideally cation-permselective membrane. This lack of ideality is a consequence of the relatively large tubule inside diameter and the very high salt concentration (1 M) used.[1]

In concentration-cell-based detection this "baseline" membrane potential of +95 mV is analogous to the baseline current obtained in the constant-potential cell. When analyte species are added to the low concentration (10^{-5} M KCl) side of the concentration cell, the membrane potential changes from this baseline value, and the change in membrane potential, ΔE, increases with the concentration of the analyte added. Figure 6 shows this effect for the addition of a cationic analyte ($Ru(bpy)_3^{2+}$) and an anionic analyte (tetraphenyl borate, TPB^-). Note that addition of the cationic analyte causes the membrane potential to decrease, and addition of the anionic analyte causes the membrane potential to increase. This suggests that the cationic analyte partially depolarizes the Au nanotubules, perhaps by ion-pairing with the chemisorbed Cl^-. In contrast, the anionic analyte apparently increases the adsorbed surface charge.

If analyte is added to the high concentration (1 M KCl) side, no change in membrane potential is observed.

Figure 7 shows results of experiments aimed at optimizing the concentration of salt used on the low concentration side of the membrane. Concentration cells were assembled with 1 M KCl on the high concentration side and various different concentrations of KCl (from 10^{-3} M to 10^{-7} M) on the low concentration side. The low concentration side of each concentration cell was then spiked with known concentrations of Ru(bpy)$_3^{2+}$; ΔE was measured after each addition of this analyte. These data were processed as plots of the ΔE measured for each concentration of analyte vs. the concentration of KCl on the low concentration side of the membrane (Figure 7). The objective is to identify the concentration of KCl that provides the highest ΔE for all concentrations of analyte employed. Figure 7 shows that this optimal concentration of KCl on the low concentration side is 10^{-5} M. This concentration (along with 1 M KCl on the high concentration side) was used in all subsequent investigations.

Figure 8 shows calibration curves for various analytes obtained in this optimum concentration cell, and Table II shows the corresponding detection limits. Note first that Ru(bpy)$_3^{2+}$ (again, the largest cationic analyte used) could be detected down to 10^{-10} M. Furthermore, the sensitivity to this analyte is again enormous ($\sim 4 \times 10^9$ mV M^{-1}). In contrast to the constant-potential cell (Table I), the smaller divalent cation MV^{2+} has a lower detection limit than the larger predominately monovalent quinine (Table II). This indicates that, as might be expected in a concentration cell, charge of the analyte plays a more important role in determining the detection limit than in the constant-potential cell.

At the pH of this electrolyte, the majority of the BCG is present as the monovalent anion. Table II shows that detection limits for anions are lower than for cations in this concentration-cell method. Hence, in addition to size-based selectivity the concentration-cell method shows charge-based selectivity. This may result from the

15

partial exclusion of anions from the nanotubules due to the chemisorbed Cl^-. Finally, all detection limits were higher (worse) when the same concentration cell was assembled but 1 M and 10^{-5} M KI were used instead of the corresponding Cl^- salts. This is undoubtedly a reflection of the lower chemisorption valence of I^- relative to Cl^-.[13,14]

DISCUSSION

At first glance, the constant-potential device would appear to function in a similar fashion as the well known Coluter® Counter used to count biological cells and colloidal particles.[6] In the Coluter® Counter a current is passed through a glass capillary, and the voltage drop across the capillary is measured. When the particle to be counted enters the capillary, the capillary is partially occluded. This results in a spike in the trans-capillary voltage, and in this way the particle is counted. Similarly, it might be suggested that when the analyte species enters the nanotubes in the constant-potential device, the nanotubes are partially occluded, and this is what is responsible for the decrease in the trans-membrane current.

However, the volume of a single nanotubule is on the order of 10^{-19} L. If this volume were allowed to completely equilibrate with a 10^{-10} M analyte solution, there would be approximately one analyte molecule in every 10^6 nanotubes. This would clearly not bring about a change in the trans-membrane current. Therefore, a response mechanism that entails bulk uptake of the analyte species by the nanotubes does not seem likely. We suggest, alternatively, that the response is surface-based, whereby collisions of the analyte molecules with the nanotube-membrane surface result in transient blockage of the mouths of the nanotubes. However, it is clear that the analyte must partially enter the mouth of the nanotube; if this were not the case, there would be no optimum nanotube size for each of the three analytes investigated in Figure 4.

We suggest the following tentative model for the response of this device: First, it is important to point out that there is electro-osmotic flow of solution from the anode half-cell (where the analyte is added) to the cathode half-cell[6]. This serves to drive the

16

analyte species to the membrane surface and to focus the analyte molecules to the tubule mouths where the flow is occurring. Second, we have shown that the diffusion coefficients for large molecules in these tubules can be as much as two orders of magnitude lower than in the bulk solution phase[15]. This is a well-known phenomenon and is explained by the theory of hindered diffusion in micropores[16]. According to this theory the flux, J, of a molecule in a flowing stream of solution within such a micropore is given by

$$J = -K^{-1} D_\infty \, \partial c/\partial x + GVC \qquad (1)$$

where K is a hydrodynamic coefficient that describes the enhanced (relative to free solution) drag experienced by the molecule in the micropore, and G is an analogous parameter that accounts for the fact that the velocity of the molecule in the micropore lags behind the fluid velocity, V, far downstream or upstream from the molecule; D_∞ is the diffusion coefficient for the molecule in free solution, $\partial c/\partial x$ is the concentration gradient, and C is the concentration of the molecule[16]. The key point of Equation 1 is that due to the influence of K and G, both the diffusion coefficient[15] and velocity of the molecule in the micropore are significantly reduced relative to these parameters in the solution phase.

We tentatively suggest that fast solution-phase diffusive- and convective-transport of analyte to the nanotubule mouth is followed by dramatically hindered diffusion and convection from the mouth into the interior of the nanotubule. As a result, the analyte molecules act as plugs that partially occlude the mouths of the tubules, and this causes the observed drop in the trans-membrane current. The current-time response (Figure 2) would then be associated with the gradual plugging of the nanotubule mouths in this way.

This tentative model appears to circumvent the problem of having too few analyte molecules to fill the complete volume of all (or even a small fraction, *vide supra*) of the nanotubules. However, is it reasonable to assume that enough molecules can be

17

brought from bulk solution to the membrane surface to plug the mouths of the nanotubules in this way? The following first-order analysis, which considers only the diffusive part of the flux, shows that the answer is yes.

The Einstein-Smoluchowski equation shows that during the five-minute response time of the device, molecules from as far away as 0.0548 cm in the solution can diffuse to the membrane surface. From the known membrane area, this gives a volume element sampled by the membrane during the measurement of 0.017 mL. Assuming 100 mL of 10^{-10} M analyte solution, there are $\sim 6 \times 10^{12}$ molecules in the entire solution, and $\sim 1 \times 10^9$ molecules in the volume element sampled by the membrane. Finally, from the known pore density and membrane area, it is easy to show that there are 2×10^8 nanotubules that need to be plugged. Hence, this simple analysis, which considers only diffusion to the membrane surface, suggests there are 5 analyte molecules for every nanotubule mouth that needs to be plugged. The enhanced mass-transport and focusing of the analyte to the mouths caused by electro-osmotic flow would only improve on this ratio.

The Langmurian shape of the calibration curve (inset Figure 3A) might also support this molecular-plugging argument. A similar shape is observed for enzyme-based sensors where there are a limited number of sites (enzyme molecules) for binding of the analyte species (17). If the nanotubule mouths are likewise considered as sites for trapping of the analyte, a calibration curve similar to the enzyme sensor might be expected.

However, this model is very preliminary. Further experimentation and modeling will be required before the mechanism of response of these devices can be clearly elucidated.

CONCLUSIONS

We have described here two new and general ways to detect analyte species in solution. Both are based on nanotubule membranes with tubule inside diameters of ~1

18

to ~3 nm. The first method involves applying a constant potential across the membrane and measuring the drop in trans-membrane current upon addition of the analyte. The second involves a concentration cell based on such membranes and measurement of the change in the membrane potential upon addition of the analyte. Both methods favor analytes of large size and higher charge. The detection limits obtained can be extremely low (e.g., 10^{-11} M for the constant-potential method). Hence, these new methods can compete with even the most sensitive of modern analytical methods, e.g., fluorescence.

These methods can, in principle, be used to detect any large analyte species. Furthermore, as was illustrated in Figure 4, the size of the analyte to be detected can be selected by selecting the appropriate nanotubule inside diameter. Hence, varying the nanotubule inside diameter is one route for building chemical selectivity into these devices. Our membrane-transport studies show that it should also be possible to introduce chemical selectivity into these devices.[3]

Table I. Detection limits obtained using the constant-potential method. The membrane contained ~2.8 nm-diameter tubules.

Cell	Analyte	Detection limt (M)
Pt/KF	$Ru(bpy)_3^{2+}$	10^{-9}
Ag/AgCl/KCl	$Ru(bpy)_3^{2+}$	10^{-10}
	Quinine	10^{-8}
	MV^{2+}	10^{-6}
	2-napthol	10^{-6}
Ag/AgI/KI	$Ru(bpy)_3^{2+}$	10^{-11}
	Quinine	10^{-8}
	MV^{2+}	10^{-7}
	2-napthol	10^{-6}

Table II. Detection limits obtained using the concentration-cell detection method. Double-junction Ag/AgCl reference electrodes and KCl electrolyte were used.

Analyte	Detection limt (M)
$Ru(bpy)_3^{2+}$	10^{-10}
MV^{2+}	10^{-9}
Quinine	10^{-8}
BCG	10^{-7}
TPB^-	10^{-7}

References

(1) Nishizawa, M.; Menon, V. P.; Martin, C. R. *Science* **1995**, *268*, 700-702.

(2) Jirage, K. B.; Hulteen, J. C.; Martin, C. R. *Science* **1997**, *278*, 655-658.

(3) Hulteen, J. C.; Jirage, K. B.; Martin, C. R. *J. Amer. Chem. Soc.*, **1998**, *120*, 6603-6604.

(4) Martin, C. R. *Science*, **1994**, *266*, 1961-1966.

(5) Menon, V. P.; Martin, C. R. *Anal. Chem.* **1995**, *67*, 1920-1928.

(6) Kobayashi, Y.; Martin, C. R. *J. Electroanal. Chem.* **1997**, *431*, 29-33.

(7) Petzny, W. J.; Quinn, J. A. *Science* **1969**, *166*, 751-753.

(8) Liu, C. Ph. D. Thesis, Texas A&M University, College Station, TX (**1991**).

(9) Sawyer, D. T.; Sobkowiak, A.; Roberts, Jr. J. L. *Electrochemistry for Chemists, 2nd Ed.*; John Wiley & Sons, Inc.: New York, **1995**; Chap. 5.

(10) Biggs, S.; Mulvaney, P.; Zukoski, C. F. Grieser, F. *J. Am. Chem. Soc.* **1994**, *116*, 9150-9157.

(11) Deakin, M. R.; Li, T. T.; Melroy, O. R. *J. Electroanal. Chem.* **1988**, *243*, 343-351.

(12) Skoog, D. A.; Leary, J. J. *Principles of Instrumental Analysis, 4th Ed*; Saunders College Publishing: Orlando, FL, 1992; Chap. 1.

(13) Bravo, B. G.; Michelhaugh, S. L.; Soriaga, M. P.; Villegas, I; Suggs, D. W.; Stickney, J. L. *J. Phys. Chem.* **1991**, *95*, 5245-5249.

(14) McCarley, R. L.; Bard, A. J. *J. Phys. Chem.* **1991**, *95*, 9618-9620.

(15) Jirage, K.B. Unpublished results Colorado State University, January, 1999.

(16) Deen, W.M. *AIChEJ*, **1987**, *33*, 1409-1425.

(17) Ballarin, B.; Brumlik, C. J.; Lawson, D. R.; Liang, W.; Van Dyke, L. S.; Martin, C. R. *Anal. Chem.*, **1992**, *64*, 2647-2651.

Figure Captions

Figure 1. Chemical structures and approximate sizes of the analytes used.

Figure 2. Plots of current vs. time after addition of $Ru(bpy)_3^{2+}$ (concentrations indicated) to the anode half-cell of a Ag/AgCl/KCl cell. The membrane contained ~2.8 nm-diameter Au nanotubules. The Au surface layers have been removed.

Figure 3. Plot of Δi versus concentration of $Ru(bpy)_3^{2+}$ (closed circle), quinine (closed triangle), or MV^{2+} (open circle) in the anode half-cell. Membrane as per Figure 2. A. Ag/AgCl/KCl cell. B. Ag/AgI/KI cell. Inset in Figure 3A shows the lowest three concentrations plotted in a non-log-log format.

Figure 4. Plot of detection limit versus nanotubule diameter for $Ru(bpy)_3^{2+}$ (closed circle), MV^{2+} (open circle) and quinine (closed triangle). Cell as per Figure 3B.
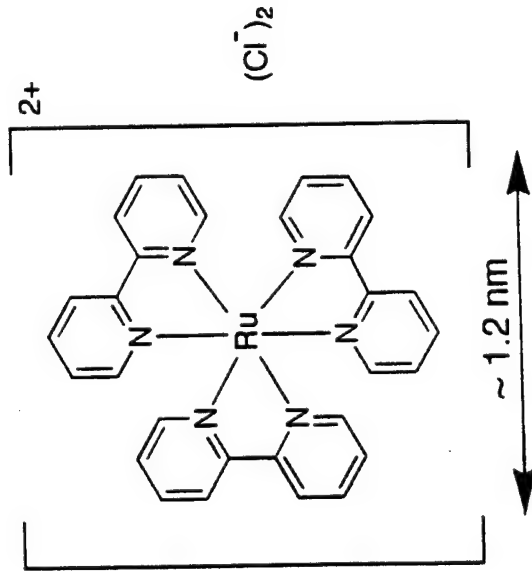
Figure 5. A. Plots of Δi versus concentration of $Ru(bpy)_3^{2+}$ (closed circle), quinine (closed triangle) or MV^{2+} (open circle) in the anode half-cell in the presence of 10^{-4} M pyridine. B. Plot of Δi versus concentration of $Ru(bpy)_3^{2+}$ in the anode half-cell in the presence of 10^{-4} M MV^{2+}. Membrane as per Figure 2. Cell as per Figure 3B.

Figure 6. Change in membrane potential in the concentration cell upon addition of 0.1 mL of 10^{-4} M $Ru(bpy)_3^{2+}$ (A) or 0.1 mL of 10^{-3} M TPB⁻ (B) to the low concentration half-cell. The KCl concentrations in the half-cells were 1 and 10^{-5} M. Membrane as per Figure 2.
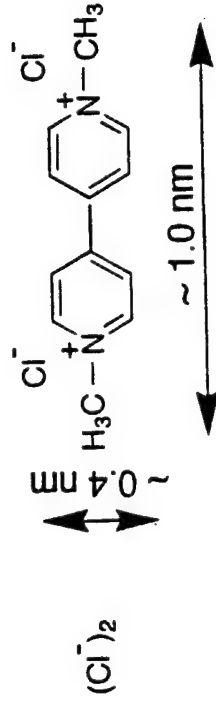
Figure 7. Plot of ΔE versus KCl concentration in the low concentration half-cell. KCl concentration in the high concentration half-cell was 1 M. The analyte was $Ru(bpy)_3^{2+}$. $Ru(bpy)_3^{2+}$ concentrations were 10^{-10} M (closed circle), 10^{-9} M (open circle), 10^{-8} M (closed triangle), 10^{-7} M (open triangle) and 10^{-6} M (closed square). Membrane as per Figure 2.

Figure 8. Plot of ΔE versus concentration of analyte in the low concentration half-cell. KCl concentrations were 1 M and 10^{-5} M. Analytes were $Ru(bpy)_3^{2+}$ (closed circle), MV^{2+} (open circle), quinine (closed triangle), BCG (open triangle) and TPB^- (closed square). Membrane as per Figure 2.
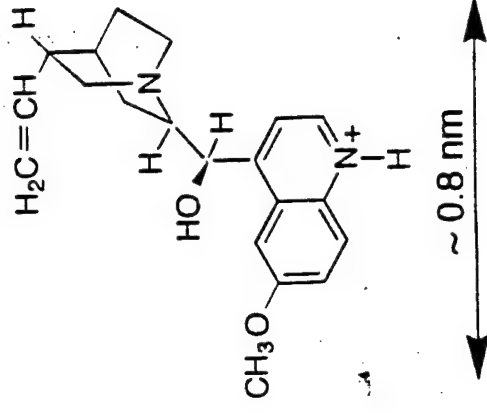
Quinine
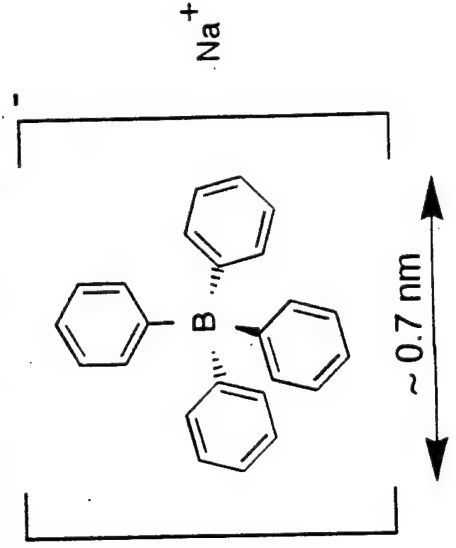
~0.8 nm

2-Naphthol

~0.7 nm

~0.5 nm

Methyl viologen

~1.0 nm

~0.4 nm

Sodium tetraphenylborate

~0.7 nm

Ru(bpy)$_3$Cl$_2$

~1.2 nm

Bromocresol Green

~0.9 nm

A
10⁻¹⁰ M

$\updownarrow$ 50 nA

B
10⁻⁸ M

$\updownarrow$ 200 nA

C
10⁻⁶ M

$\updownarrow$ 1000 nA

Δi

Current (arb. units)

0   1   2   3   4   5

Time (min)

Concentration (M)

|Δi| (nA)

Inset axes:
|Δi| (nA)
600
300
0
Concentration of Ru(bpy)$_3^{2+}$ (×10^9 M)
0 1 2 3 4 5 6 7 8 9 10

Concentration (M)

$|\Delta i|\ (nA)|$

Concentration (M)

$| \Delta i$ (nA) $|$

Fig 5B

Concentration of Ru(bpy)$_3^{2+}$ (M)

| Δi (nA)|

Fig. 5